Late Stage Dynamics of Phase Separation Processes of Binary Mixtures Containing Surfactants

doi: 10.1063/1.466213

Late stage dynamics of phase separation processes of binary mixtures containing surfactants

Toshihiro Kawakatsu[a] and Kyozi Kawasaki
Department of Physics, Faculty of Science, Kyushu University 33, Fukuoka 812, Japan

Michihiro Furusaka
BSF, National Laboratory for High Energy Physics, Tsukuba 305, Japan

Hirofumi Okabayashi
Department of Applied Chemistry, Nagoya Institute of Technology, Nagoya 466, Japan

Toshiji Kanaya
The Institute for Chemical Research, Kyoto University, Uji 611, Japan

(Received 15 June 1993; accepted 5 August 1993)

Late stage dynamics of phase separation processes of immiscible binary mixtures containing surfactants (amphiphilic molecules) is investigated by computer simulations on the hybrid model proposed by the present authors [T. Kawakatsu and K. Kawasaki, Physica A **167**, 690 (1990)]. With use of this hybrid model, one can investigate large scale phenomena while retaining the intramolecular structures of surfactant molecules. Simulations are performed both for irregular bicontinuous and micellar domain formation processes taking the thermal fluctuation effects into account. In the very late stage, the coarsening of the domain structures is considerably slowed down both for bicontinuous and micellar domain formation processes due to the low interfacial tension of the surfactant–adsorbed interfaces. Scaled scattering structure functions are also calculated, which possess the characteristic features of the experimentally observed scattering functions of microemulsions and polymer blends containing amphiphilic block copolymers. We found that the calculated structure function for the system containing surfactants is different from that for the simple binary mixture without surfactant. Also reported are the important effects of thermal fluctuations on micellar domain structures, where the domain formation is considerably accelerated by the thermal fluctuation.

I. INTRODUCTION

Recently, more and more attentions have been being focused on the slow relaxation processes in complex systems.[1,2] Dynamics of glasses, polymer melts and microemulsions, which are generally called "complex fluids," are well-known examples.[2] Although simple theoretical approaches to such problems, like scaling arguments by de-Gennes,[3] give us a conceptually important understanding of the systems, various complications associated with the complex fluids have been preventing us from obtaining quantitative understanding of the phenomena in microscopic and mesoscopic scales. Computer simulation methods, which have become very popular in the last decade in the field of complex fluids, are a powerful tool to attack such complex problems.

We have been investigating the dynamics of binary mixtures containing surfactants, such as microemulsions or polymer blends containing amphiphilic block copolymers, using several computer simulation techniques; the hybrid model proposed by the present authors,[4–6] a Monte Carlo simulation of a spin model,[7,8] and a molecular dynamics simulation of a molecular model.[8] The hybrid model, which is discussed in detail in the present paper, is a phenomenological semimicroscopic model, where the binary mixture and the surfactant are treated as continuous field and discrete molecules, respectively. Using the above-mentioned three models, we have mainly investigated the early stage dynamics of the phase separation processes in the presence of surfactants. We also investigated the late stage dynamics using the hybrid model. Since the model is based on a coarse-grained picture, it allows us to simulate long time behavior of large scale systems.

In this paper, taking such advantages of the hybrid model, we extensively investigate the late stage dynamics of the phase separation processes in the presence of surfactants in detail. We also include the effects of thermal fluctuations in this work. Recently, Laradji *et al.* performed a computer simulation on the similar problem.[9] In their works, they adopted a pure continuum description, where both the binary mixture and the surfactant are described by two continuous fields,[10] and therefore the microscopic details of the surfactant molecules, e.g., the molecular size or the head-to-tail ratio, are averaged out in their model. On the contrary, the main advantage of our hybrid model is that the model can directly take the molecular details of the surfactant into account. We have shown that such molecular details of the surfactant cannot be neglected in the early stage of phase separation processes, especially for large surfactants like block copolymers.[6] The effects of the molecular details of the surfactant also appear in the late stage of the phase separation through the mechanical properties of the surfactant adsorbed interfaces, such as the bending elasticity of the interface, and the spontaneous

[a]Author to whom correspondence should be addressed.

 0021-9606/93/99(10)/8200/18/$6.00

curvature of the surfactant–adsorbed interfaces due to the head to tail unbalance of the surfactant molecule.[11] Such features can easily be taken into account in the hybrid model.[12] Therefore, the hybrid model can be applied both for the early stage dynamics and the late stage dynamics with a reasonable computational efficiency.

Although there have been very few real experiments on the surfactant effects on the dynamics of phase separation processes, some attempts have just been started recently using polymer blends and amphiphilic block copolymers.[13,14] Such polymer blends/block copolymer systems are suitable targets of our hybrid model as will be mentioned in Sec. II and in Appendix A, and it is a crucial test for the hybrid model to compare the results of our simulations, which will be given in the present paper, with those of the real experiments.

This paper is organized as follows. In the next section, we describe the hybrid model briefly and introduce thermal fluctuation effects into the model. We also give a brief review of the results obtained in our previous works.[4–8] In Sec. III, the results of the computer simulations on the late stage dynamics are shown, which are discussed in connection with the other relevant simulations[9] and experiments.[13,14] We also give an intuitive explanation for the results of the simulation. Various characteristic time scales associated with the coarsening process are discussed in Sec. IV and the results are compared with those of the real experiments using polymer blends and block copolymers. Finally, we conclude our results in Sec. V.

II. THE HYBRID MODEL

In this section, we describe the hybrid model briefly and give a summary of the results obtained so far by the computer simulations and analytical treatments using this model. In the present work, we include the thermal fluctuation into our hybrid model, which were entirely neglected in our previous works.[4–6]

We consider an immiscible binary mixture, whose components are denoted as A and B, and surfactant molecules immersed in the binary mixture. In general, a surfactant molecule in an A/B binary mixture consists of an A-philic part and a B-philic part, and therefore the surfactant molecule has an amphiphilic nature. Now, we consider *a large surfactant molecule* in comparison with the molecules of the binary mixture. For example, readers can imagine an amphiphilic block copolymer molecule solubilized in a binary mixture composed of molecules with a relatively low molecular weight (For possible experiments using polymers which correspond to the situation discussed in the present paper are given in Appendix A.) Such a separation in length scales of the sizes of the molecule of the binary mixture and the surfactant molecule allows us to describe the binary mixture and the surfactant in different manners. In the hybrid model, the binary mixture is described by a continuous scalar field $X(\mathbf{r})$ which is defined as

$$X(\mathbf{r}) \equiv \rho_A(\mathbf{r}) - \rho_B(\mathbf{r}), \tag{2.1}$$

where $\rho_A(\mathbf{r})$ and $\rho_B(\mathbf{r})$ are the densities of the A and the B components of the binary mixture at a position $\mathbf{r}$. On the other hand, the surfactant is described by discrete molecules each of which has a spin variable called a director, i.e., a unit vector pointing the direction from the B-philic center to the A-philic center. A surfactant molecule is specified by its position $\mathbf{r}_i$ and its director $\hat{\mathbf{s}}_i$, i being the index of the surfactant molecule.

These variables $X(\mathbf{r})$, $\mathbf{r}_i$ and $\hat{\mathbf{s}}_i$ are assumed to obey the following phenomenological equations of motion, which are purely dissipative:

$$\frac{\partial}{\partial t} X(\mathbf{r},t) = L^X \nabla^2 \frac{\delta H}{\delta X(\mathbf{r})} + f(\mathbf{r},t), \tag{2.2}$$

$$\frac{d}{dt} \mathbf{r}_i(t) = -L^\rho \frac{\partial H}{\partial \mathbf{r}_i} + \mathbf{g}_i(t), \tag{2.3}$$

$$\frac{d}{dt} \hat{\mathbf{s}}_i(t) = -L^s \left[\frac{\partial H}{\partial \hat{\mathbf{s}}_i} - \left(\frac{\partial H}{\partial \hat{\mathbf{s}}_i} \cdot \hat{\mathbf{s}}_i \right) \hat{\mathbf{s}}_i \right] + \mathbf{h}_i(t). \tag{2.4}$$

Equation (2.2) is the so-called time dependent Ginzburg–Landau model and Eqs. (2.3) and (2.4) are equations of motion for a particle moving in a viscous medium and we have temporarily neglected hydrodynamic interactions, which can be justified for a two-dimensional system of a thin fluid layer placed between two parallel glass plates (Helle–Shaw cell, see Appendix A). Of course, such a hydrodynamic interaction cannot be neglected for a three-dimensional system and should be included in a standard manner.[15] In Eqs. (2.2)–(2.4), L^X, L^ρ, and L^s are Onsager coefficients, H is the total free energy functional and $f(\mathbf{r},t)$, $\mathbf{g}_i(t)$ and $\mathbf{h}_i(t)$ thermal fluctuations which obey the following fluctuation–dissipation relations:

$$\langle f(\mathbf{r},t) f(\mathbf{r}',t') \rangle = -2L^X T \nabla^2 \delta(\mathbf{r}-\mathbf{r}') \delta(t-t'), \tag{2.5}$$

$$\langle \mathbf{g}_i(t) \mathbf{g}_j(t') \rangle = 2L^\rho T \delta_{ij} \delta(t-t') \mathbf{1}, \tag{2.6}$$

$$\langle \mathbf{h}_i(t) \mathbf{h}_j(t') \rangle = 2L^s T \delta_{ij} \delta(t-t') (\mathbf{1} - \hat{\mathbf{s}}_i \hat{\mathbf{s}}_i). \tag{2.7}$$

The other cross-correlations are vanishing because of our neglection of the cross-couplings in Eqs. (2.2)–(2.4). In Eqs. (2.5)–(2.7), T is the temperature measured in unit of the Boltzmann's constant k_B, and $\mathbf{1}$ is the unit tensor. The thermal fluctuation on the field $X(\mathbf{r})$ becomes negligible in the late stage of the phase separation where the system is divided into large domains separated by sharp interfaces. The same is true for the noise on the surfactant molecules in our hybrid model, because the surfactant molecule is regarded as a meso-scale object which has also been coarse-grained on the same length scale as that of the field $X(\mathbf{r})$ (see Appendix A). On the other hand, in the early stage, the thermal fluctuation on both the field $X(\mathbf{r})$ and surfactant molecules cannot be neglected and it plays an important role on the dynamics of the phase separation.[16] Since we are interested in both early stage and late stage of the phase separation processes, we here included the thermal fluctuations on the field $X(\mathbf{r})$ and on the surfactant molecules. Note also that the temperature T can vary independently of the quench depth, the temperature difference between the temperature of the system under consideration

and the critical temperature. For example, thermal fluctuation is negligible for polymer blends,[17] while it cannot be neglected for systems consisting of molecules with low molecular weights.[18]

Total free energy functional H is the same as that used in our previous works,[4–6] whose explicit expressions are given as the following:

$$H=H_{XX}+H_{XS}+H_{SS}, \tag{2.8}$$

$$H_{XX}=\int d\mathbf{r}\left[\tfrac{1}{2}D_X(\nabla X)^2-\frac{c}{2}X^2+\frac{u}{4}X^4\right], \tag{2.9}$$

$$H_{XS}=\mu_S N_S+\frac{ql}{2}\sum_i\int d\mathbf{r}V_-(\mathbf{r}-\mathbf{r}_i)\hat{\mathbf{s}}_i\cdot\nabla X(\mathbf{r}), \tag{2.10}$$

$$H_{SS}=q^2\sum_{i<j}\left[2V_+(r_{ij})+\frac{l^2}{4}(\mathbf{s}_{ij}^-\mathbf{s}_{ij}^-):\nabla\nabla\phi(r_{ij})+\frac{l^2}{4}(\mathbf{s}_{ij}^+\mathbf{s}_{ij}^+):\nabla\nabla\psi(r_{ij})\right], \tag{2.11}$$

where D_X, c, u, μ_S, q, and l are positive constants, N_S is the total number of surfactant molecules in the system, $\mathbf{s}_{ij}^{\pm}\equiv\hat{\mathbf{s}}_i\pm\hat{\mathbf{s}}_j$ and $r_{ij}\equiv|\mathbf{r}_i-\mathbf{r}_j|$, l is the measure of the linear dimension of the surfactant molecule, q is the measure of the strength of the interaction between a surfactant molecule and the binary mixture, and c is the measure of the quench depth. $\phi(r)$ and $\psi(r)$ are interaction potentials between surfactant molecules and the field X, where $\phi(r)$ is the attractive interaction between chemically similar parts and $\psi(r)$ is the repulsive interaction between chemically dissimilar parts, and $V_{\pm}(r)\equiv\phi(r)\pm\psi(r)$. We assume the functional forms of ϕ and ψ as,

$$\phi(r)=-\alpha\exp(-r/\xi),\qquad \psi(r)=\beta\exp(-r/\xi). \tag{2.12}$$

In deriving Eqs. (2.8)–(2.11), we assumed that the surfactant molecule is symmetric with respect to the exchange between its A-part and the B-part [an extension to an asymmetric case can easily be done (Ref. 12)], and we neglected the excluded volume effects of the surfactant molecule, which is expected not to be important in the late stage of the phase separation where the interfacial region becomes negligibly small. [The effects of the excluded volume of the surfactant molecule cannot be neglected in the early stage (see Refs. 6 and 7).] Intuitive explanations of the terms in H_{XS} and H_{SS} are as follows: the first term on the right-hand side (r.h.s.) of Eq. (2.10) is the chemical potential of the surfactant molecule and the second term accounts for the attractive interaction between surfactant molecules and interfaces, where $|\nabla X|$ is large. The first term on the r.h.s. of Eq. (2.11) is the interaction between centers of mass of two surfactant molecules. As two surfactant molecules cannot completely overlap due to the excluded volume interaction, the potential V_+ should be repulsive at a short distance. In order to take such an excluded volume effect into account phenomenologically we assume that $\beta>\alpha$ in Eq. (2.12), although the values of α and β should in principle be determined from the microscopic considerations (Appendix A). Such a repulsive interaction leads to the saturation of interfaces by the adsorbed surfactant molecules in the late stage of the coarsening process. The second and the third terms on the r.h.s. of Eq. (2.11) account for the bending elasticity of the interface onto which surfactant molecules are adsorbed.

In our previous publications, we performed computer simulations on the hybrid model but neglected the thermal fluctuations.[4–6] We succeeded in reproducing typical domain structures, e.g., irregular bicontinuous, micellar, lamellar and bilayer structures, depending on the composition of the binary mixture and the number density of the surfactant.[4,5] The early stage dynamics of the phase separation has been investigated both analytically and by computer simulations.[6] We found that the phase separation is assisted by the added surfactant when the size of the surfactant molecule is comparable to the natural wavelength of the early stage phase separation (i.e., correlation length of the binary mixture). Such an assistance is due to the amphiphilic effects of the surfactant molecule, which plays the role of a nucleus for the phase separation.[6] This feature was confirmed by molecular dynamics simulations on binary soft-sphere systems containing an amphiphilic block copolymer chain.[8] On the other hand, when the surfactant molecule is small compared to the wavelength of the phase separation, the surfactant molecules can be regarded as impurities, which decelerate phase separation.[6] Such a deceleration was confirmed by Monte Carlo simulations on a spin system containing small surfactant molecules.[7]

In the above-mentioned results on the early stage dynamics, the main feature of the surfactant molecule, i.e., the role of lowering the interfacial tension, does not play a role because of the absence of sharp interfaces in the system. However, it is obvious that such a role of lowering the interfacial tension is extremely important in the late stage of phase separation, where the phase separation dynamics is dominated by the motion of interfaces driven by the interfacial tension. In the next section, we present the results of the computer simulations on the late stage dynamics of phase separation processes. In our previous work,[6] a slowing down of the phase separation in the late stage has been observed for micellar formation processes, which originates from the saturation of the surfactant molecules on the interfaces. However, we could not observe such a slowing down in the bicontinuous case, where the total length of interfaces (the system used in our simulation is two-dimensional) is much longer than the micellar case and the saturation of the interfaces by surfactant molecules has not been achieved yet. Therefore, it is necessary to perform longer computer simulations with a larger system size in order to confirm the validity of our hybrid model in the late stage of phase separation processes.

III. RESULTS OF COMPUTER SIMULATIONS

We have performed extensive computer simulation runs using the hybrid model to investigate the late stage dynamics of formation processes of irregular bicontinuous structures and micellar structures starting from uniformly

mixed initial states. We investigate two cases, one is the case without thermal fluctuation and the other is the case including thermal fluctuation. In the following, we present the results of these simulations for bicontinuous case and micellar case, separately.

Computer simulations are performed in the same way as the previous works,[4–6] but with an improved computing efficiency by introducing an "implicit method" described in Appendix B to solve the partial differential equation for the field $X(\mathbf{r})$. The system is a two-dimensional square box with periodic boundary conditions imposed on each side and is divided into 256×256 square meshes with a mesh size $a=0.3$ to calculate the field $X(\mathbf{r})$. The effects of the thermal fluctuation are calculated using the standard method.[19–21] The parameters used are the same as those used in our previous works; $D_X=c=u=1.0$, $L^X=0.09$, $L^\rho=5.0$, $L^s=1.0$, $q=0.1$, $l=1.0$, $\alpha=1.0$, $\beta=5.0$, and $\xi=1.0$, respectively. Three choices of the temperature T was used, $T=0.0$, 0.01, and 0.1. The unit of the temperature is taken to be the Boltzmann's constant, which has the same order as the interfacial free energy per unit length (correlation length) of the binary mixture.

Initial state for the computer simulation was chosen as a completely mixed state of the binary mixture and surfactant molecules. As the initial configuration for the field $X(\mathbf{r})$, we used uncorrelated Gaussian random numbers with a mean X_0 and a standard deviation 0.2, X_0 taking the value 0 for the bicontinuous case and -0.5 for the micellar case. Note that X_0 denotes the total composition of the system and is conserved during the simulation run.

The introduction of the implicit method allows us to choose a larger time mesh Δt than the explicit scheme without causing any instabilities of the computational scheme. However, a selection of too large Δt changes the time scale although the qualitative features of the solution are kept unchanged. (A further discussion on this problem is given in Appendix B.) As we are interested only in the qualitative features of the model in this work, we selected rather large Δt, that is $\Delta t=0.5$, in order to cover a longer time regime from the early stage to the very late stage. (This selection of Δt causes a change in the time scale by a factor of 3.6.) For the bicontinuous case, ten independent runs were performed up to $t=2000.0$ (4000 iterations) and usually five independent runs were performed up to $t=25\,000.0$ (50 000 iterations), respectively. For the micellar case, we performed five independent runs up to $t=10\,000.0$ (20 000 iterations). The data shown in the following are averaged over these independent runs. The time regime covered by the present simulation runs is 7–20 times longer than that of the previous simulations.[4]

In order to show the effects of added surfactant systematically, we performed several simulation runs changing the number of surfactant molecules, i.e., $N_S=0$, 2048, and 4096, which correspond to the total number density of the surfactant ρ_S as $\rho_S=0.0$, 0.347, and 0.694, respectively. All the other parameters and initial configurations for the field $X(\mathbf{r})$ are set to be unchanged.

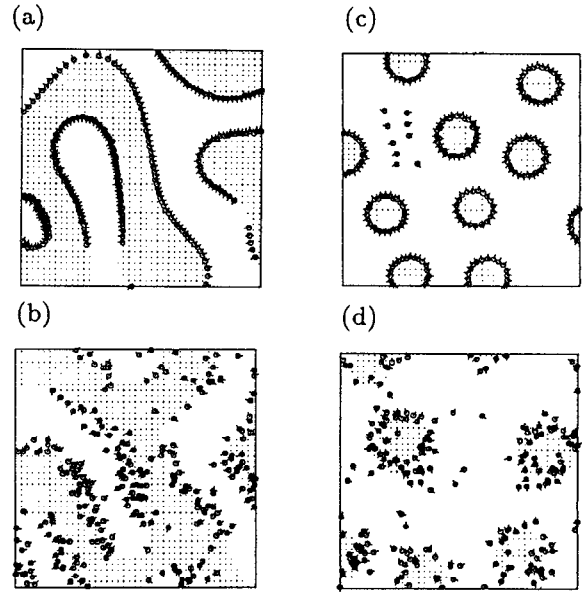

FIG. 1. Snapshot pictures of the system (1/9 of the total simulation box) obtained by the computer simulations for irregular bicontinuous structures (a) $T=0.0$ and (b) $T=0.1$, and for micellar structures (c) $T=0.0$ and (d) $T=0.1$, respectively. All pictures are taken at $t=2000.0$ for $\rho_S=0.347$. Dotted and white regions correspond to A-rich domains and B-rich domains, respectively, and the surfactant molecule is shown by a small circle with a short line.

A. Domain structures

Figure 1 shows the snapshot pictures of the system obtained by the computer simulations for the four typical cases, i.e. (a) the irregular bicontinuous case without thermal fluctuations ($X_0=0.0$ and $T=0.0$); (b) the irregular bicontinuous case with thermal fluctuations ($X_0=0.0$ and $T=0.1$); (c) the micellar case without thermal fluctuations ($X_0=-0.5$ and $T=0.0$); (d) the micellar case with thermal fluctuations ($X_0=-0.5$ and $T=0.1$). In all these figures, the surfactant number density is taken to be $\rho_S=0.347$. Each snapshot picture is a part of the total system (1/9 of the total area) at $t=2000.0$. Dotted regions and white regions correspond to A-rich domains and B-rich domains, respectively, and the surfactant molecules are shown by small circles each with a short line directed along $-\hat{\mathbf{s}}_i$. In cases (a) and (b), the A-domains and the B-domains are separated by surfactant layers and are mutually interconnected in a irregular manner. Such a structure is called the irregular bicontinuous structure. In cases (c) and (d), the minor phase (A-phase) forms small globules covered by surfactant molecules, which are normally called micelles.

In the absence of the thermal fluctuation effects [(a) and (c)], one can confirm that almost all the interfaces have already been covered by adsorbed surfactant molecules, which form regularly-aligned single layers on the interfaces. This result shows that the time range covered by our previous simulations[4–6] are too short to reach the final configuration, especially for the bicontinuous case, because surfactant molecules still formed clusters on interfaces in the previous simulations (see Fig. 3 in Ref. 4).

On the other hand, for the case with thermal fluctuation effects [(b) and (d)], surfactant molecules no longer form regularly-aligned single layers although most of the surfactant molecules are adsorbed onto interfaces. In these cases, surfactant molecules can easily be exchanged between different parts of interfaces due to the activation by the thermal fluctuation. Such an activation never occurs in the case with $T=0$ and, therefore, all the surfactant molecules are trapped onto interfaces and cannot escape from the interfacial region. This point is particularly crucial for the micellar case, where the number of surfactant molecules in each micelle cannot change without activation processes and it becomes difficult for the system to escape from a metastable configuration. In the bicontinuous case, this is not so serious because interfaces are mutually connected and the surfactant molecules can diffuse along interfaces, which allows the density of surfactant molecules on interfaces to change easily. This point will later be discussed in detail.

We should note the fact that the temperature T is a measure of the importance of the thermal fluctuation in the phase separation process and can be greatly different from system to system. One might imagine that the case Fig. 1(b) can be achieved by heating the system in Fig. 1(a); this is not correct. The quench depth, which is measured by the parameter c in Eq. (2.9), is much sensitive to the temperature change than the parameter T itself and therefore heating the system greatly changes this parameter c, which can totally alter the situation of the phase separation process. Therefore, the case with finite T should be regarded as a different system from the case with $T=0$. For example, the case $T=0$ can be regarded as a polymer system[17] while the case $T>0$ corresponds to a system consisting of molecules with low molecular weights, like critical binary fluids.[18]

B. Dynamics of formation processes of irregular bicontinuous structures

In this section, we consider formation processes of irregular bicontinuous structures, that is, the case with the equal volume fractions of the A and the B components of the binary mixture [Figs. 1(a) and 1(b)].

1. The case without thermal fluctuations

First we discuss the case without thermal fluctuations ($T=0.0$). In Fig. 2, we show snapshot pictures of the total system at $t=2\,000.0$ and $20\,000.0$ for cases (a) $\rho_S=0.0$; (b) $\rho_S=0.347$; and (c) $\rho_S=0.694$, respectively. (As we will see below, both $t=2\,000.0$ and $20\,000.0$ are in the late stage of the phase separation.) Here the system is too large to distinguish each surfactant molecule. They are shown by black stripes on the A/B-interfaces.

One can recognize the differences in the domain structures between Figs. 2(a)–2(c). In the case of a simple binary mixture without surfactant [Fig. 2(a)], the domain structure is kept self-similar during a long time period, which is the origin of the dynamical scaling. However, when we add the surfactant [Figs. 2(b) and 2(c)], the domain structures seem to be time-dependent. In the later

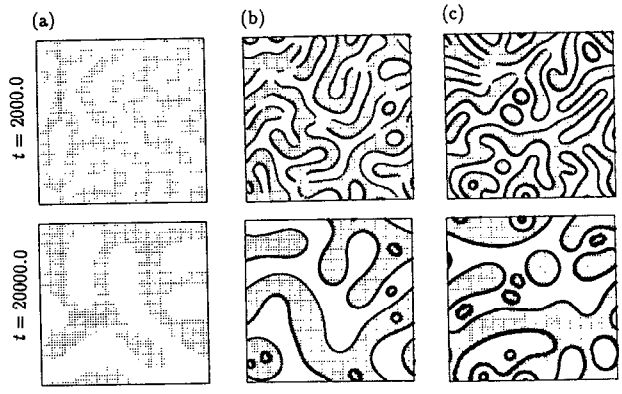

FIG. 2. Snapshot pictures of the total system at $t=2\,000.0$ and $20\,000.0$ for the bicontinuous cases ($T=0.0$) with (a) $\rho_S=0.0$; (b) $\rho_S=0.347$; and (c) $\rho_S=0.694$, respectively. Surfactant molecules are shown by black stripes on the A/B-interfaces.

time regime, there appear considerable number of small micelles in large domains, because the micelles are stabilized by the surfactant layer surrounding themselves. This can lead to a breakdown of the dynamical scaling for the system with added surfactant. In the absence of such surfactant layers, the micelles are not long-lived and will disappear through the evaporation–condensation process.

In order to discuss the phase separation process quantitatively, we calculated the circularly averaged scattering structure function of the field $X(\mathbf{r})$, denoted as $S(k,t)$, which is defined as

$$S(k,t)=\frac{1}{2\pi}\int_0^{2\pi}d\theta\int d\mathbf{r}\langle X(\mathbf{r},t)X(\mathbf{0},t)\rangle\exp(i\mathbf{k}\cdot\mathbf{r})$$
$$\equiv\frac{1}{2\pi}\int_0^{2\pi}d\theta S(\mathbf{k},t), \tag{3.1}$$

where θ is the angle between the wave vector $\mathbf{k}$ and an arbitrarily chosen base direction, $k\equiv|\mathbf{k}|$, L is the side length of the system and $S(\mathbf{k},t)$ is the noncircularly averaged scattering function. In Fig. 3, temporal evolutions of $S(k,t)$ calculated from the simulation data are shown for (a) $\rho_S=0.0$; (b) $\rho_S=0.347$; and (c) $\rho_S=0.694$, respectively. These scattering functions are calculated during the time interval ranging from the early stage to the late stage ($0.0\leqslant t\leqslant 2000.0$) and are averaged over ten independent runs. As is expected for coarsening systems, the peak of $S(k,t)$ shifts to the smaller wave number side with its peak height also increasing. Note that as was discussed in our previous papers,[5,6] the growth of $S(k,t)$ is accelerated in the early stage by adding surfactant molecules. Also one can confirm that the initial peak position shifts to the higher wave number side as the concentration of the added surfactant is increased.[5,6]

In order to see the coarsening process in the late stage more clearly, we calculated the characteristic wave number. The characteristic wave number $\langle k(t)\rangle$, the inverse of which is a measure of the average domain size, is defined as

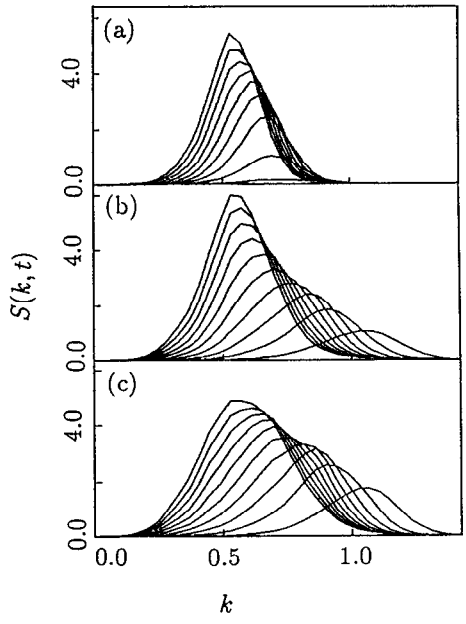

FIG. 3. Temporal evolutions of the structure function $S(k,t)$ calculated from the simulation data (averaged over ten independent runs) are shown for bicontinuous cases ($T=0.0$) with (a) $\rho_S=0.0$; (b) $\rho_S=0.347$; and (c) $\rho_S=0.694$, respectively. Times are, from bottom to top, $t=0.0$, 200.0,...,2000.0, respectively.

$$\langle k(t)\rangle = \int_0^\infty kS(k,t)dk \Big/ \int_0^\infty S(k,t)dk$$

$$= \int S(\mathbf{k},t)d\mathbf{k} \Big/ \int |\mathbf{k}|^{-1}S(\mathbf{k},t)d\mathbf{k}, \qquad (3.2)$$

where we have used the definition of $S(\mathbf{k})$ in Eq. (3.1) in the second line. In Fig. 4, we show the temporal change of $\langle k(t)\rangle$ in double-logarithmic plot. The data are averaged over five independent runs, except for the case $\rho_S=0.694$ where the data are obtained from three independent runs.

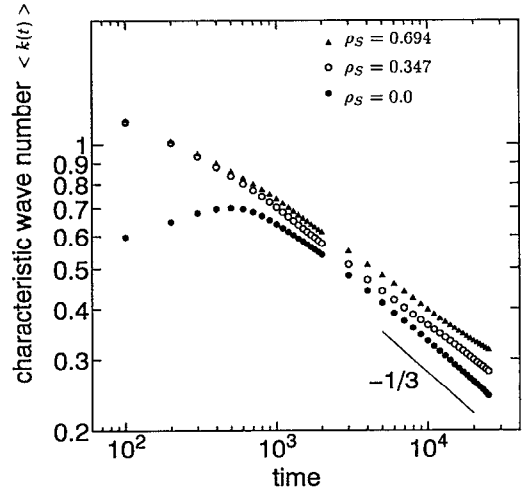

FIG. 4. Temporal changes of the characteristic wave number $\langle k(t)\rangle$ for various surfactant densities are shown in a double logarithmic scale for the bicontinuous case ($T=0.0$). Data for $\rho_S=0.0$ and 0.347 are averaged over five runs, while the data for $\rho_S=0.694$ are averaged over three runs.

For the case without the surfactant ($\rho_S=0.0$), there are two different time regimes. The first one is the so-called linear regime. In this linear regime, the characteristic wave number does not change and only the peak height of $S(k,t)$ grows. Such a behavior is shown in Fig. 4 as a plateau around $t<500.0$. After this linear regime, $\langle k(t)\rangle$ decreases proportionally to $t^{-1/3}$ due to the nonlinear effects. Such an exponent, $-1/3$, is well-known for the spinodal decomposition in binary mixtures without the hydrodynamic interaction.[22]

For the case with added surfactant ($\rho_S=0.347$ and 0.694), one can observe that the added surfactant have remarkable effects on the dynamics. In this case, the linear regime appears to be too short to be observed in Fig. 4. As was discussed in our previous papers,[5,6] the initial peak starts to grow at a higher wave number than that for the case without surfactant and the growth of the peak height of $S(k,t)$ is considerably enhanced [see also Figs. 3(b) and 3(c)]. Thus, in the early stage, a sharp domain structure is already formed for the case with surfactant but the spatial pattern itself is much more fine-grained than the case without surfactant. After this initial stage, one can see that $\langle k(t)\rangle$ decreases as $t^{-1/3}$ also for the case with surfactant, which means that the domain growth is dominated by the interfacial tension as in the usual spinodal decomposition. In this regime, the surface tension is of course reduced by the adsorbed surfactant molecules but it is not so low as to alter the growth exponent. However, in the late stage, a slowing down of the phase separation can be seen especially for the case with a higher surfactant density ($\rho_S=0.694$) and the growth exponent gradually changes to a slower value than 1/3. Such a slowing down originates from the decrease in the interfacial tension of the surfactant–adsorbed interfaces.

The gradual change from the $t^{-1/3}$ regime to the final slowing-down regime can be understood by an effect of the interfacial tension, where the interfacial tension is usually a monotonously decreasing function of the surfactant density on the interface.[23] As the coarsening process proceeds, the total length of interfaces decreases and the average surfactant density on the interfaces increases, which results in the lowering of the interfacial tension. Noting the fact that the interfacial tension is the main driving force of the domain growth in the usual spinodal decomposition processes without surfactant,[24] such a decrease in the interfacial tension leads to a slowing down in the coarsening of the domain structure. (An intuitive explanation of this behavior is given in Sec. III C.) When the surfactant molecules are adsorbed onto interfaces and the interfacial tension becomes small compared with the bending free energy of the interface, the bending energy can affect the dynamics of interfaces. Such a possibility is also considered in Sec. IV.

Actually, such a slowing down of the coarsening and the branching of the curves in the late stage shown in Fig. 4 have been observed in a real experiment using a polymer blend containing an amphiphilic block copolymer.[14] We should note that in a real three-dimensional polymer blend,

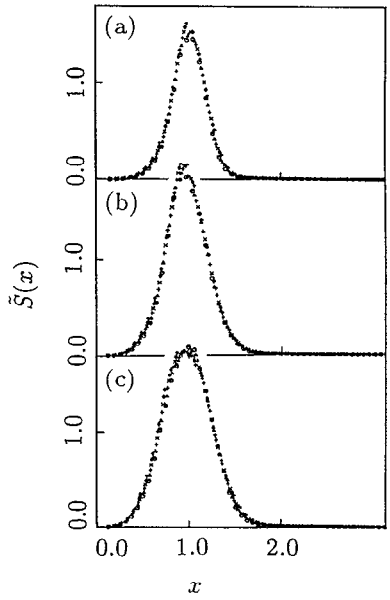

FIG. 5. Scaled structure functions $\tilde{S}(x)$ are shown for the bicontinuous case ($T=0.0$) with (a) $\rho_S=0.0$; (b) $\rho_S=0.347$; and (c) $\rho_S=0.694$, respectively. Data are plotted for $t=1500.0$, 1600.0,...,2000.0 (averaged over ten runs).

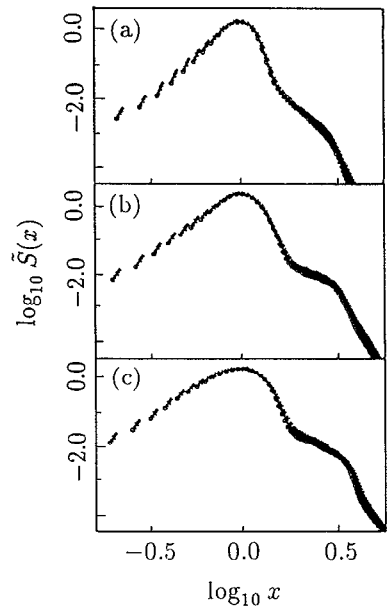

FIG. 6. Scaled structure functions in Fig. 5 are plotted in double logarithmic scales.

the coarsening process proceeds not as $\langle k(t)\rangle \sim t^{-1/3}$ but as $\langle k(t)\rangle \sim t^{-1}$ due to the hydrodynamic interaction.[15]

Recently Laradji *et al.* performed computer simulations on a similar problem and reported that they did not observe the behavior $\langle k(t)\rangle \sim t^{-1/3}$ but a behavior $\langle k(t)\rangle \sim -\ln t$ before equilibration.[9] Such a logarithmic time regime, which is slower than the $t^{-1/3}$ growth, can be identified with the final slowed-down regime in our simulation results. The transient $t^{-1/3}$ regime may be too short to be observed in their system.

The characteristic features of the domain structure can well be extracted by calculating the scaled scattering function, $\tilde{S}(x)$, which is defined through the following relation:

$$S(k,t)=\langle k(t)\rangle^{-d}\tilde{S}[k/\langle k(t)\rangle], \tag{3.3}$$

where d is the dimensionality of the system. We show the calculated scaling functions in Fig. 5, each being averaged over ten independent runs. As the functional form of the scaling function is sensitive to the finite size effects of the system, we used the data in the time period $1500.0 \leqslant t \leqslant 2000.0$, which is at the beginning of the late time regime (see Fig. 4). Even for the case with the surfactant, all the data lie on a single master curve, which can be a sign of the existence of the dynamical scaling. Such a dynamical scaling property for the surfactant system was also reported by Laradji *et al.*[9] We should note that the time interval used to calculate the data in Fig. 5 is not so long enough to insist that Fig. 5 shows the dynamical scaling. As the scaling function is sensitive to the finite size effects of the system, the data in the very late stage cannot be used to discuss the functional form of the scattering function due to the small system size used in our simulations.

To discuss the details of the functional forms of these scaling functions, it is useful to plot these functions on double-logarithmic scales. Such plots are shown in Fig. 6. One can observe a shoulder at $x=3$ ($\log_{10} x=0.477$) for all cases (a)–(c). Such a shoulder is actually observed in real experiments on microemulsions and is regarded as a sign of local ordering in the domain structures, for example, local lamellar structures.[25] We should note here that such a shoulder is not unique in the surfactant systems but is widely seen in spinodal decomposition phenomena.[22,26]

We found that in case (c) this shoulder becomes less pronounced at the later time while in case (a) the shoulder remains. To show this, we present the scaled scattering function calculated at $t=2000.0$ and 3000.0 in Fig. 7. One can observe that the scaling function is time dependent especially in case (c) and the bump is becoming less and less noticeable in the later time, which indicates that the dynamical scaling does not hold strictly in this time regime for the case with the surfactant. One can understand this from Fig. 2, where the morphology of the domain structure changes and the distribution of the domain width becomes more and more random as time goes on.

The most important feature of the scaled scattering functions in Fig. 6 is that the main peak becomes broader when we add the surfactant into the binary mixture. This broadening of the main peak shows that the configuration of the interfaces becomes more random when the surfactant is added. When the surfactant molecules are adsorbed onto interfaces, the surfactant molecules form almost incompressible fluid layers on the interfaces, which prevent the interfaces from shrinking. This is of course the origin of the slowing down of the coarsening in the late stage, and moreover, such surfactant fluid layers cause undulations of the interfaces, which leads to the broadening of the main peak.[27]

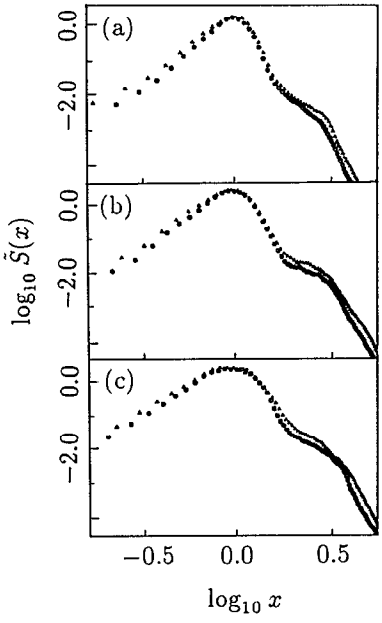

FIG. 7. Scaled structure functions at later times (t=2000.0 and 3000.0). Data shown are averaged over five runs in (a) and (b) and over three runs in (c).

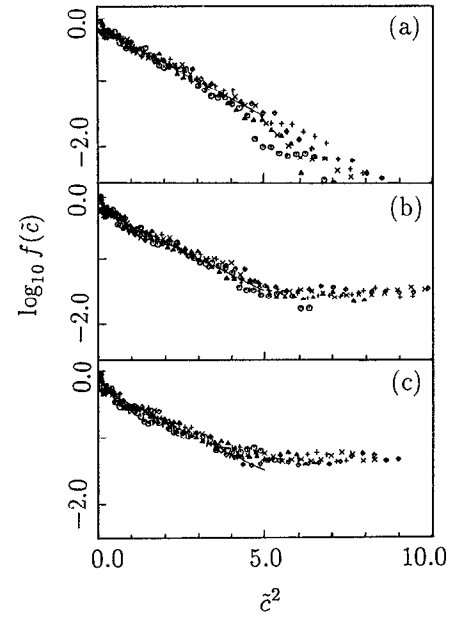

FIG. 9. Normalized curvature distribution functions $f(\tilde{c})$ in a logarithmic scale as a function of square of a scaled curvature, $\tilde{c}$, defined as $\tilde{c} \equiv c[L^2/l_p(t)]^{-1}$, c being the unnormalized interfacial curvature. Data are averaged over the time interval 4 000.0$\leq t \leq$12 000.0. Data for ρ_S=0.0 and 0.347 are averaged over five runs, while the data for ρ_S=0.694 are averaged over three runs.

So far, we have concentrated on the data in the Fourier space. In the following we turn our attention to the real space analyses. An important quantity to characterize the growth of the domain structure, which can be calculated in the real space, is the perimeter length $l_p(t)$ which is defined as the total length of interfaces in the system. We show the temporal evolution of $l_p(t)$ in Fig. 8, which shows a similar behavior to that of $\langle k(t) \rangle$ in Fig. 4. Actually, the quantity $L^2/l_p(t)$ (L is the side length of the system) is often used as a characteristic length of the domain structure instead of $2\pi/\langle k(t) \rangle$, because $L^2/l_p(t)$ is proportional to the average domain size. In this figure, one can see a crossover from $l_p(t) \sim t^{-1/3}$ regime to $l_p(t) \sim t^{-\alpha}$ ($0 < \alpha < 1/3$) regime which is similar to that in Fig. 4. The slightly different behavior of $l_p(t)$ from that of $\langle k(t) \rangle$ in Fig. 4 originates from the fact that the perimeter length $l_p(t)$ is less sensitive to the finite size effects of the system than the characteristic wave number $\langle k(t) \rangle$. From Fig. 8, one finds that the perimeter length at the onset of the slowing down of the domain growth takes the value $\sim$1500.0 for the case ρ_S=0.694 and $\sim$1200.0 for the case ρ_S=0.347, respectively. The values of the average separation distance between surfactant molecules on the interface calculated from these perimeter length values are 0.38 for the case ρ_S=0.694 and 0.6 for the case ρ_S=0.347, both of which are the same order as the interaction range of the surfactant molecule. This indicates that the slowing down of the domain growth takes place when the entire interface is fully saturated by surfactant molecules, which prevent the interface from shrinking due to the repulsive interaction between adjacent surfactant molecules.

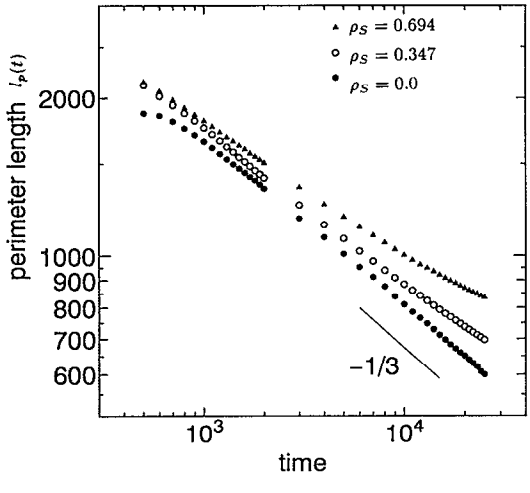

FIG. 8. Temporal evolution of the perimeter length $l_p(t)$ for bicontinuous case (T=0.0) are shown in double logarithmic scales. Data for ρ_S =0.0 and 0.347 are averaged over five runs, while the data for ρ_S=0.694 are averaged over three runs.

Another important information on the domain configuration in real space is the interfacial curvature, because the curvature is the main driving force for the coarsening. Moreover, the bending energy of the interface, which is normally written in a quadratic form of the curvature,[28] has an important contribution to the equilibrium interfacial configuration in microemulsions.[29] It may also be possible to measure the interfacial curvature in microemulsions by scattering experiments.[30] We calculated the curvature distribution using the method described in the Appendix C. In Fig. 9, we show the normalized curvature distribution function $f(\tilde{c})$ in a logarithmic scale as a function of square of a scaled curvature, $\tilde{c}$, which is defined as

$\tilde{c} \equiv c[L^2/l_p(t)]^{-1}$, c being the unnormalized interfacial curvature. Here, the distribution function is normalized as $\int_0^\infty f(\tilde{c})d\tilde{c}=1$ and the data during $4\,000.0 \leqslant t \leqslant 12\,000.0$ are superposed on the figure. This normalized curvature distribution function should be time invariant for the simple binary mixture without surfactant [Fig. 9(a)] because of the existence of the dynamical scaling and the self-similar nature of the domain structure. One can actually observe a master curve in case (a). The linear dependence in case (a) shows that $f(\tilde{c})$ is a Gaussian function of $\tilde{c}$. We also find an almost time invariant functions in the cases (b) and (c), the cases with added surfactant. At the smaller curvature region, one can also observe a linear dependence, which shows the Gaussian distribution, similar to the case without surfactant. However, at the larger curvature region, there is a plateau, which shows that there are considerable short range undulations of interfaces due to the adsorbed surfactant effects. The crossover points from the linear part at small curvature region to the plateau at larger curvature region in cases (b) and (c) are at about (b) $c \sim 0.38$ and (c) $c \sim 0.34$ (both are unscaled curvatures), respectively. Therefore the plateau at larger curvature region indicates interfacial undulations with a radius of curvature $R \sim 3.0$. In Figs. 2(b) and 2(c), we find many small micelles and small wavelength undulations of the interfaces whose characteristic lengths are the same order as the radius of curvature $R \sim 3.0$ obtained above. Such micelles and small undulations are not so frequent for the case without the surfactant [Fig. 2(a)]. This result corresponds to the broadening of the main peak of the scattering function shown in Fig. 6(c). We evaluated the slope of the linear part at small curvature region and obtained the values (a) -0.28 ± 0.01; (b) -0.26 ± 0.01; and (c) -0.26 ± 0.01. Therefore, the slopes are the same for these three cases. This means that the large scale domain structure is essentially insensitive to the existence of the added surfactant and only small scale structure is changed. This may be due to the fact that our simulation runs have not yet reached the final stage where the interfacial tension vanishes due to the adsorbed surfactant and the domain structure is frozen (see Figs. 4 and 8).

At present, we do not know the origin of the Gaussian form of the curvature distribution because the present system is far from equilibrium. If the system is in equilibrium, the Gaussian distribution can be expected by considering the two-dimensional analog of the interfacial free energy functional proposed by Helfrich;[28]

$$H_{\text{int}} = \int ds \left[\sigma + \frac{\kappa}{2} c(s)^2 \right], \tag{3.4}$$

where s is the natural coordinate, i.e., the contour length along the interface, σ is the interfacial tension, $c(s)$ is the curvature at point s on the interface, and κ is the bending modulus of the interface. [For a more general case with an asymmetry between the A-species and the B-species, e.g., the case of a surfactant with head to tail unbalance, $c(s)$ in Eq. (3.4) should be replaced by $c(s)-c_0$, where c_0 is the spontaneous curvature.] The expression Eq. (3.4) is also valid for three-dimensional case, where the line curvature $c(s)$ is replaced by the mean curvature, as long as there is no topological changes in the domain structure. [In the presence of topological changes, one has to add the Gaussian curvature term to Eq. (3.4).] In the equilibrium state, one finds that the Helfrich free energy Eq. (3.4) leads to the Gaussian distribution of the curvature as a result of the equipartition relation. On the other hand in the present situation, the system is far from equilibrium and one cannot assume the equipartition relation. However, the Gaussian form of the curvature distribution may suggest a possible relation between the equilibrium statistics of the interfacial configuration and that of a growing domain pattern. For example, the Gaussian distribution of the curvature may indicate that the small wavelength undulations of interfaces are already equilibrated while the large scale domain structure is still growing.

The result shown in Figs. 9(b) and 9(c) indicates that there are two different length scales in the system for the case with the surfactant, one is the domain size and the other is the short wavelength undulations of interfaces. As is easily understood, the latter length scale is rather time-independent in the late stage and cannot be scaled in the same manner as the domain size. This suggests that the dynamical scaling does not hold until the domain size becomes much larger than the persistence length. Another possibility for the scaling nature to hold is the case where the growth of the domain stops at a certain time. In this case, we will have a frozen domain structure rather than a growing self-similar domain structure.

In microemulsions, the persistence length is of the same order as the domain size due to the very low interfacial tension,[31] and we expect that one cannot get a dynamical scaling in the formation processes of microemulsions. In this sense, we cannot interpret the data shown in Fig. 5 with the dynamical scaling in strict manner. Actually, in the presence of the added surfactant, we observed that the scattering function changes its functional form as the coarsening proceeds (see Figs. 6 and 7).

2. The case with thermal fluctuations

We also performed a series of simulation runs on the irregular bicontinuous structures with thermal fluctuation effects ($T=0.1$). In the late stage of the phase separation process, the results are almost the same as those for the case without thermal fluctuations presented in the previous subsection. Therefore, we will give only a summary of the results for this case.

In Fig. 10, we show the temporal evolution of the perimeter length $l_p(t)$ for different surfactant densities. The behavior is in almost *quantitatively* agreement with that of the case $T=0.0$ (Fig. 8). We also calculated the scaled scattering function for these cases, and the results are shown in Fig. 11 in double-logarithmic plots. The data presented are calculated during the same time interval as that in Fig. 6. Again the overall properties of the scaled scattering function are similar to those in Fig. 6.

From these results, we concluded that the thermal fluctuation does not play an important role in the late

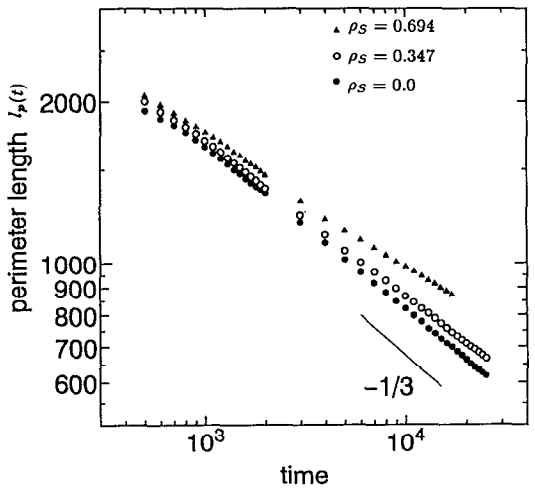

FIG. 10. Same as Fig. 8, but for the case with thermal noise ($T=0.1$). Data for $\rho_S=0.0$ and 0.347 are averaged over five runs, while the data for $\rho_S=0.694$ are averaged over two runs.

stage dynamics of the phase separation process of the bicontinuous case.

C. Intuitive explanation for the bicontinuous case

In this section we give simple explanation of the behavior of the characteristic length $l(t)$ (or the characteristic wave number $\langle k(t)\rangle$ which is related to $l(t)$ by the relation $l(t)\sim 2\pi/\langle k(t)\rangle$) for the formation processes of irregular bicontinuous structures based on a simple dimensional analysis. The argument does not depend on the dimensionality of the system.

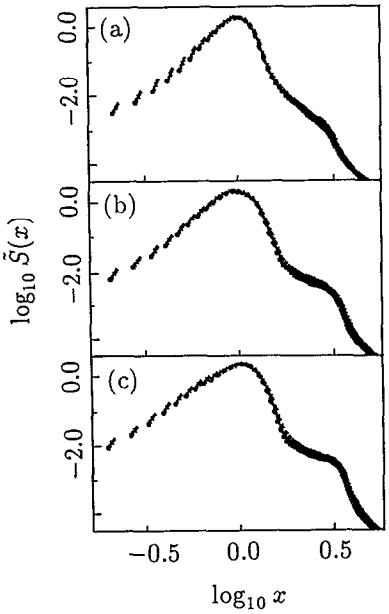

FIG. 11. Scaled scattering functions for the bicontinuous cases with thermal noise ($T=0.1$). (a) $\rho_S=0.0$; (b) $\rho_S=0.347$; and (c) $\rho_S=0.694$, respectively. Data are plotted for $t=1500.0$, 1600.0,...,2000.0 (averaged over ten runs).

Following Kawasaki and Ohta,[24] the velocity of the interface normal to itself, $v(\mathbf{a})$, at the point $\mathbf{a}$ on the interface is given by the curvature of the interfaces through the following relation:

$$(2X_e)^2 \int d\mathbf{a}' G[\mathbf{r}(\mathbf{a}),\mathbf{r}(\mathbf{a}')]v(\mathbf{a}') = L^X \Sigma(\mathbf{a}) c_m(\mathbf{a}), \tag{3.5}$$

where X_e is the equilibrium value of the filed $X(\mathbf{r})$ defined using the coefficients in Eq. (2.9) as $X_e^2 \equiv c/u$, $\mathbf{a}$ is the coordinate specifying the point on the interface [for a one-dimensional interface embedded in a two-dimensional space, the coordinate $\mathbf{a}$ reduces to the natural coordinate s used in Eq. (3.4)], $\mathbf{r}(\mathbf{a})$ is the position of the point specified by the coordinate $\mathbf{a}$, $\Sigma(\mathbf{a})$ and $c_m(\mathbf{a})$ are the interfacial tension and the mean curvature of the interface at $\mathbf{a}$, respectively, and $G(\mathbf{r},\mathbf{r}')$ is the Green's function of the diffusion field which satisfies

$$-\nabla^2 G(\mathbf{r},\mathbf{r}') = \delta(\mathbf{r}-\mathbf{r}'). \tag{3.6}$$

Assuming that there is only one characteristic length scale in the system, i.e., $l(t)$, we apply a simple dimensional consideration to find $v(\mathbf{a})\sim dl(t)/dt$ and $c_m(\mathbf{a})\sim 1/l(t)$, respectively. Substituting these relations into Eq. (3.5), we obtain

$$\frac{d}{dt} l(t) \sim \frac{L^X}{(2X_e)^2} \langle \Sigma(t)\rangle l(t)^{-2}, \tag{3.7}$$

where $\langle \Sigma(t)\rangle$ is the interfacial tension averaged over the interfaces.

It is well-known that the interfacial tension of surfactant–adsorbed interfaces is a function of the surfactant density on the interface.[23,32] Let σ_S and $\Sigma(\sigma_S)$ be the surface density of surfactant molecules on the interface and the corresponding interfacial tension. As long as the surfactant density is low, the interfacial tension is a linear function of σ_S,

$$\Sigma(\sigma_S) = \Sigma_0[1-\gamma\sigma_S], \tag{3.8}$$

where Σ_0 is the bare interfacial tension of the interface onto which no surfactant molecules are adsorbed and γ is some constant which should be determined from the microscopic details of the system.[23,32] The same behavior as Eq. (3.8) can also be obtained from the hybrid model.[5]

On the other hand, the decrease in the interfacial tension stops by saturation when the surfactant density exceeds some critical value, which corresponds to the so-called critical micelle concentration. In microemulsions, such a saturated value of the interfacial tension is almost vanishing, which is the origin of the thermodynamic stability of microemulsions.[31] Noting these two limiting behaviors, we make the following ansatz for the interfacial tension:

$$\Sigma(\sigma_S) = \Sigma_0 \exp(-\sigma_S/\sigma_S^0), \tag{3.9}$$

where σ_S^0 is the saturation density of the surfactant molecules. The exponential functional form of the above ansatz is nothing but a one possible interpolation between the two

limits $\sigma_S \ll \sigma_S^0$ and $\sigma_S^0 \ll \sigma_S$. The assumed functional form at large σ_S can affect the final result as is discussed in the following.

Using the ansatz, Eq. (3.9), we can estimate $\langle \Sigma(t) \rangle$ in Eq. (3.7). If almost all the surfactant molecules are adsorbed onto interfaces, the average surfactant density on interfaces is expressed as $\langle \sigma_S \rangle \sim l(t)$. Using this estimate and Eq. (3.9), we obtain

$$\langle \Sigma(t) \rangle \sim \Sigma_0 \exp[-l(t)/l^0], \tag{3.10}$$

where l^0 is the value of $l(t)$ where the saturation of surfactant molecules on the interfaces occurs. Substituting Eq. (3.10) into Eq. (3.7) leads to a closed equation for $l(t)$, which can be solved easily to give the following results:

$$l(t) \sim t^{1/3} \quad [l(t) \ll l^0]$$
$$\sim \ln t \quad [l^0 \leqslant l(t)]. \tag{3.11}$$

This result shows that the phase separation process proceeds in the same manner as the usual spinodal decomposition as long as the surfactant density on the interfaces are not so large. However, when the surfactant molecules become saturated on the interfaces, the growth exponent changes gradually from 1/3 to 0, the latter being the asymptotic behavior of the logarithmic function, and the domain structure is frozen or equilibrated asymptotically. Therefore, we conclude that the logarithmic behavior observed by Laradji *et al.*[9] corresponds to a transition from the $t^{1/3}$ regime to the final frozen (or equilibrium) regime. Also note that the logarithmic behavior in Eq. (3.11) originates from the ansatz, Eq. (3.9), where the functional form of the interfacial tension is assumed to be an exponential one. The logarithmic behavior in Eq. (3.11) has nothing to do with any activation processes while the usual logarithmic behavior in phase separation processes in the presence of moving impurities originates from a kind of activation process.[33]

D. Formation of micellar structures

In the previous subsections, we studied the bicontinuous case, where effects of the thermal fluctuation on the phase separation process were minor. Here we show results of another important case, i.e., the micellar formation processes. We will show importance of effects of the thermal fluctuation in such micellar formation processes.

We performed computer simulation runs for the case with the composition of the binary mixture $A:B=1:3$ (i.e., $X_0=-0.5$), for temperatures $T=0.0$, 0.01, and 0.1, respectively. In these simulations, we can observe micellar formation processes whenever surfactant molecules are added. However, within the same time regime, we could not observe any appreciable phase separations in the case without surfactant molecules. This fact shows that the uniformly mixed state of the binary mixture at this composition is almost metastable when there is no surfactant added. (Using the mean-field approximation, one can show that the parameter point is very close to the spinodal line, which is a boundary between the metastable region and the unstable region in the phase diagram.) As was mentioned

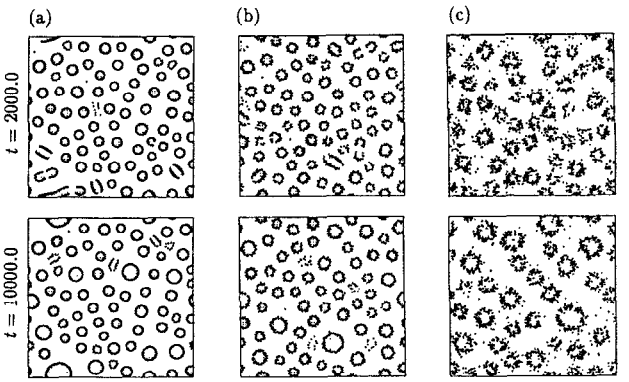

FIG. 12. Snapshot pictures of the total system at $t=2\,000.0$ and 10 000.0 for the micellar cases with $\rho_S=0.347$ and with (a) $T=0.0$; (b) $T=0.01$; and (c) $T=0.1$, respectively.

in our previous works,[5,6,8] the added surfactant molecules play the role of nuclei and initiate the phase separation process when the molecular size is at least comparable to the correlation length of the phase separating binary mixture. In the following, we give results only for the cases with $\rho_S=0.347$, where all data are averaged over five independent runs.

Snapshot pictures of the system in the late stage of the phase separation process are shown in Fig. 12 for cases (a) $T=0.0$; (b) $T=0.01$; and (c) $T=0.1$, respectively, at $t=2\,000.0$ and 10 000.0. As was reported previously,[4] local triangular-lattice structures of circular micelles with almost same sizes are formed in the case without thermal fluctuation at $t=2000.0$ [Fig. 12(a)]. However, such triangular-lattice structures are easily destroyed by thermal fluctuation [Fig. 12(c)]. Moreover one can observe that the shape and the size of the micelles are greatly altered by thermal fluctuation. In order to show this more clearly, we calculated the distribution functions of the micellar radius, which are scaled by the average micellar radius and the results are shown in Fig. 13. The data are averaged over the time interval $5\,000.0 \leqslant t \leqslant 10\,000.0$ and also over five independent runs. Figure 13 shows that the micelles are more or less monodispersed in the absence of the thermal fluctuation [Fig. 13(a)] while they are rather polydispersed under the thermal fluctuation [Figs. 13(b) and 13(c)]. Such a difference originates from the activation due to thermal fluctuation. As the added surfactant shifts the critical temperature upwards, the system is brought into the spinodal region, because the phase point of the binary mixture was originally close to the spinodal line. Thus the phase separation process is initiated similarly to the spinodal decomposition (bicontinuous case) mentioned in the previous subsections, leading to an emergence of an almost spatially periodic composition fluctuations, which later grow to be the micelles. Therefore, the initial micellar size distribution is almost monodisperse. However, in the presence of thermal fluctuation, the micellar size distribution gradually becomes polydisperse due to exchanges of surfactant molecules between micelles. Note that the activation process is crucial for the domain growth in this mi-

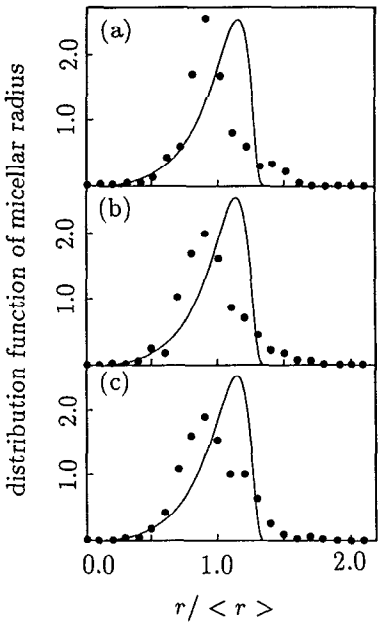

FIG. 13. Scaled and normalized micellar radius distribution functions. The horizontal axis is scaled by the average micellar radius. Data shown are averaged over the time interval $5\,000.0<t<10\,000.0$ and also averaged over five runs. The solid curve is the theoretical prediction for a two-dimensional Ostwald ripening without surfactant by Rogers and Desai (Ref. 34).

FIG. 14. Temporal evolution of the circularly averaged scattering functions for the micellar case with (a) $T=0.0$; (b) $T=0.01$; and (c) $T=0.1$, respectively. Times are from bottom to top, $t=0.0$, 500.0,...,5000.0, respectively (averaged over five runs).

cellar case, because the surfactant molecules can transfer from one micelle to another only by such activation processes.

In Fig. 13, we also show the theoretical prediction of the droplet size distribution for the two-dimensional Ostwald ripening, i.e., the case without surfactant, given by Rogers and Desai.[34] Obviously the micellar size distribution of our surfactant system is broader and more symmetric than that of the Ostwald ripening. A possible reason for the broad and symmetric distribution is the effect of the finite volume fraction of the micelles.[35,36] Another possibility is the stabilizing effect of the surfactant layer coating the micelles, which allows smaller micelles to survive for a long time and shifts the peak of the distribution function to the smaller side.

In Figs. 14 and 15, we show temporal evolutions of the circularly averaged structure function $S(k,t)$ and the characteristic wave number $\langle k(t)\rangle$, defined by Eqs. (3.1) and (3.2), respectively. The phase separation process seems to be almost frozen in the late stage in all cases. However, the resulting mean micellar radius is considerably larger in the case with a higher temperature ($T=0.1$) than that in the cases with lower temperatures ($T=0.0$ and 0.01). This is due to the activation processes mentioned above. It should be noted that the usual growth exponent $-1/3$ characterizing the Ostwald ripening process[37] cannot be observed in both cases due to the saturation of the surfactant molecules on the interfaces, which reduces the interfacial tension considerably.

From Fig. 15, one can find that the cases with $T=0.0$ and 0.01 behave in almost the same manner, which is different from that for the case with $T=0.1$. We can attribute this property to the fact that the escape events of surfactant molecules outside the micelles due to the thermal activation are essentially absent in the case $T=0.01$ [Fig. 12(b)], because the thermal noise level is much smaller than that of the attractive force between a surfactant molecule and an interface, which is of the order of unity.

Recently, Brown and Chakrabarti reported a spontaneous pinning of domain growth in off-critical binary polymer blends by computer simulation.[38] In the case of polymer blends, the thermal activation effect is largely suppressed due to the small entropic contribution from the translational degrees of freedom of polymer chains to the free energy. Thus the growth of droplets is sensitive to the

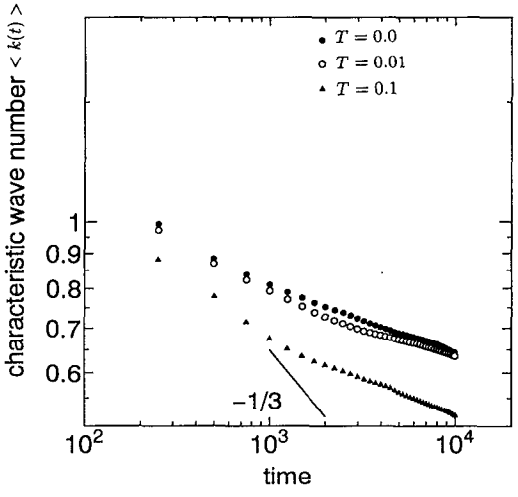

FIG. 15. Temporal evolution of the characteristic wave number $\langle k(t)\rangle$ for the micellar cases (averaged over five runs).

thermal noise. In the absence of thermal noise, they found a freezing of the droplet growth, while the droplet growth still continues in the presence of thermal noise. Such a situation is very similar to the present situation of the micellar case, which cannot be observed in the bicontinuous domain formation processes.

IV. VARIOUS CHARACTERISTIC TIME SCALES ASSOCIATED WITH THE COARSENING PROCESS

In this section, we evaluate different time scales which exist in the phase separation system under consideration. Relevant time scales which should be discussed are (1) characteristic time scale of the phase separation of the binary mixture *without* surfactant t_0; (2) time scale of the adsorption of surfactant molecules onto interfaces t_a; (3) crossover time from the regime dominated by the diffusion process to that dominated by the hydrodynamic interaction t_c; (4) the time when interfaces are saturated by surfactant molecules t_s; (5) characteristic times of the interfacial motion due to the interfacial rigidity t_r. As a particular example, we consider the bicontinuous domain formation process in a binary liquid mixture containing amphiphilic block copolymer, which is discussed in detail in Appendix A. We also evaluate the corresponding time scales in the real experiment.[14]

A. Characteristic time of the phase separation

The characteristic time scale of the phase separation of the binary mixture, t_0, is given by the growth rate of the scattering function $S(k,t)$ in the initial linear regime as[39]

$$t_0^{-1}=2\lambda(k_0)=k_0^2 D_{\rm app}, \tag{4.1}$$

where $2\lambda(k)$ is the growth rate of $S(k,t)$ in the linear regime defined by the relation $S(k,t)\sim\exp[2\lambda(k)t]$, k_0 is the initial peak position of $S(k,t)$, and $D_{\rm app}$ is the mutual diffusion coefficient of the binary mixture. Using the parameter of the hybrid model, t_0 can be rewritten as

$$t_0^{-1}=\frac{c^2 L^X}{2D}. \tag{4.2}$$

B. Time scale of surfactant adsorption

The time scale of the surfactant adsorption onto interfaces can be identified with the time scale for a surfactant molecule to diffuse over the domain size in the initial stage k_0^{-1}. If the polymerization index of the surfactant molecule (block copolymer chain) is Z_S times as that of the constituent molecule of the binary mixture, the self-diffusion coefficient of the surfactant molecule is given by $D_S=D_c/Z_S$ using the Rouse description.[3] Here, D_c is the self-diffusion coefficient of the binary mixture, which is related to the mutual diffusion coefficient $D_{\rm app}$ by $D_c=D_{\rm app}/\epsilon$,[39] where ϵ is the quench depth measured by the parameter c in Eq. (2.9). (A precise argument gives the relation $\epsilon=4c/3u$.) Then using Eq. (4.1), the characteristic adsorption time t_a is given by

$$t_a^{-1}\equiv k_0^2 D_S=\epsilon Z_S t_0. \tag{4.3}$$

Therefore, t_a is of the same order as t_0 when $\epsilon Z_S\sim 1$ holds. On the other hand, if $\epsilon Z_S\gg 1$, t_A can be much larger than t_0, and the surfactant molecules are adsorbed onto interfaces only after sharp interfaces are formed.

C. Crossover from the diffusion regime to the hydrodynamic regime

Once well-defined interfaces are formed, the interfacial motion is driven either by the diffusion process or by the hydrodynamic interaction as long as the interfaces are not saturated by the surfactant molecules. As was discussed in our previous paper,[4] a crossover from the diffusion-dominated regime to the hydrodynamics-dominated regime takes place at the time t_c given by

$$l(t_c)\sim(L^X\eta)^{1/2}/\Delta X, \tag{4.4}$$

where $l(t)$ is the average domain size at time t, η is the viscosity of the binary mixture, and ΔX is the difference between the two equilibrium values of the filed $X(\mathbf{r})$, which is given by $\Delta X=2(c/u)^{1/2}$.

Before the crossover, the coarsening process is dominated by the diffusion process and therefore using Eq. (3.7) we obtain an explicit expression for $l(t)$ as

$$l(t)\sim\left(\frac{D_{\rm app}t}{6k_0}\right)^{1/3} \quad \text{(diffusion dominated regime)}. \tag{4.5}$$

Combining Eqs. (4.4) and (4.5), t_c is given by

$$t_c=\frac{6k_0(L^X\eta)^{3/2}}{D_{\rm app}(\Delta X)^3}. \tag{4.6}$$

As was shown previously,[4] this crossover time is valid even if the driving force for the interface is not the interfacial tension but the interfacial rigidity.

After this crossover time t_c, the coarsening process is dominated by the hydrodynamic interaction. Using Eqs. (3.24) and (3.30) of Ref. 4 and neglecting the contribution from the bending rigidity, one finds that $l(t)$ is given by

$$l(t)\sim\frac{\Sigma}{\eta}t \quad \text{(hydrodynamics dominated regime)}. \tag{4.7}$$

where Σ is the interfacial tension. Equation (4.7) is valid when the interfacial tension is large compared with the bending energy of the interface.

Here, we note that the interfacial motion driven by the diffusion can be observed only in very viscous fluids like polymer melts with large molecular weights. For critical binary fluids with low molecular weights, a Brownian coagulation process is dominant instead of the diffusion controlled interfacial motion,[40] both mechanisms leading to the same $t^{1/3}$ domain growth with a coefficient which is the same order as that of Eq. (4.5).

D. Time scale of surfactant saturation

The time scale of the surfactant saturation on the interface t_s is given by

$$A(t_s)=N_S A_S, \tag{4.8}$$

where $A(t)$ is the total interfacial area at time t, N_S is the total number of surfactant molecules, and A_S is the interfacial area occupied by a surfactant molecule at the close packing density of the surfactant molecules on the interface. The total interfacial area $A(t)$ is given by the average domain size $l(t)$ as $A(t)\sim V/l(t)$, where V is the system volume. Using this relation and the definition $\rho_S=N_S/V$, one finds

$$l(t_s)=(\rho_S A_S)^{-1}, \tag{4.9}$$

where $l(t)$ is given either by Eq. (4.5) (diffusion dominated regime) or by Eq. (4.7) (hydrodynamics dominated regime).

In the case with a block copolymer as a surfactant, the molecular cross section of a surfactant molecule A_S is determined by considering a block copolymer layer adsorbed onto an interface. At the close packing density, the subchains of the block copolymer form a polymer brush adsorbed onto the interface. Denoting the height of such a brush as h_S, A_S is given by $A_S=\phi_S/(\rho_S h_S)$, where ϕ_S is the surfactant volume fraction. Substituting this relation into Eq. (4.9) leads

$$l(t_s)=\frac{h_S}{\phi_S}. \tag{4.10}$$

If $t_s<t_c$, the domain growth is dominated by the diffusion process and the l.h.s. of Eq. (4.10) should be replaced by Eq. (4.5). Therefore, we obtain

$$t_s\sim\frac{6k_0}{D_{\rm app}}\left(\frac{h_S}{\phi_S}\right)^3 \quad (t_s<t_c). \tag{4.11}$$

Otherwise, the domain growth is already dominated by the hydrodynamic interaction and we obtain using Eqs. (4.7) and (4.10)

$$t_s\sim\frac{\eta h_S}{\Sigma\phi_S} \quad (t_c<t_s). \tag{4.12}$$

E. Characteristic relaxation time due to the interfacial rigidity

Once almost all the interfaces are saturated by surfactant molecules, the interfacial motion is dominated by the bending rigidity of the interface. Using Eqs. (3.24) and (3.30) of Ref. 4 and neglecting the contribution from the interfacial tension, one obtains the interfacial velocity v as follows:

$$v\sim\frac{L^X\kappa}{(\Delta X)^2}l^{-4} \quad \text{(diffusion dominated)}$$

$$\sim\frac{\kappa}{\eta}l^{-2} \quad \text{(hydrodynamics dominated)}, \tag{4.13}$$

where κ is the bending modulus. Thus the characteristic time scale of the motion due to the bending rigidity, t_r, is given by

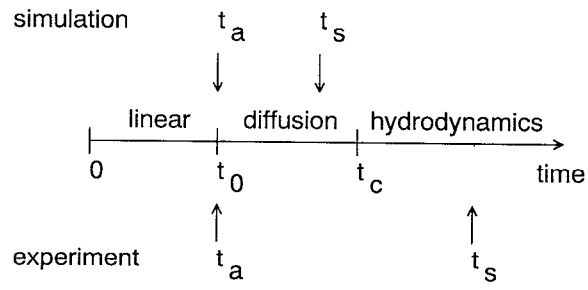

FIG. 16. A schematic representation of the various characteristic time scales both for the simulation and for the experiment is shown.

$$t_r^{-1}\sim\frac{L^X\kappa}{(\Delta X)^2}l^{-5} \quad \text{(diffusion dominated)}$$

$$\sim\frac{\kappa}{\eta}l^{-3} \quad \text{(hydrodynamics dominated)}. \tag{4.14}$$

F. Actual time scales in real experiment and computer simulation

Now, we evaluate the characteristic time scales in the real experiment done by Hashimoto and Izumitani on polymer blends containing block copolymers.[14] In their experiment, they obtained $k_0\sim 1.0\times 10^{-2}$ ($\rm nm^{-1}$), $D_{\rm app}\sim 10$ ($\rm nm^2/s$), $\epsilon\sim 2.5$, $Z_S\sim 1.0$, and $\phi_S=0.03$–0.06, respectively. As the actual value of h_S is not known to us, we assume it as the gyration radius of the block copolymer chain which is estimated as $h_S\sim 10^2$ (nm). Using these parameters, we estimate the characteristic times as $t_0\sim t_a\sim 10^3$ (s) and $t_s\sim 10^7$ (s). As we do not have the data of η and Σ, we used Eq. (4.11) to estimate t_s, although the actual domain growth is dominated by the hydrodynamic interaction in the late stage. They performed the experiment up to $t/t_0\sim 10^2$, which is far below the estimated value of t_s. Therefore, we expect that the interfaces are not yet saturated by surfactant molecules in this case. Such an prediction is justified by the experimental observation that the domains still grow although a slowing down of the coarsening due to the surfactant adsorption is observed.

The situation is almost the same for our simulation, where the saturation time t_s is much larger than the time scales of the phase separation and the adsorption, i.e., $t_0\sim t_a\ll t_s$. One difference is that the domain growth in our simulation is dominated by the diffusion process, while the domain growth in the experiment by Hashimoto and Izumitani is dominated by the hydrodynamic interaction. A schematic representation of these characteristic time scales both for the simulation and for the experiment is shown in Fig. 16.

V. CONCLUSIONS AND DISCUSSIONS

In this paper, we presented results of extensive computer simulations on the phase separation process in the presence of surfactant molecules using the hybrid model. Behavior of the scattering functions and characteristic

wave number (or characteristic length) observed in these simulations are corresponding to the experimental results and also to other simulation results. We found that there is a crossover in the temporal evolution of the characteristic length of the pattern, $l(t)$, from the usual $l(t) \sim t^{1/3}$ behavior, which characterizes the spinodal decomposition, to slower growth. Such a crossover occurs at the point where the surfactant molecules are saturated on the interfaces. We also gave an intuitive explanation of these results based on a dimensional analysis, which can successfully reproduce the observed behavior. Curvature distribution functions are also calculated from the simulation data, which show that the curvature distribution function can well be described by the Gaussian form both for the cases with and without surfactant.

We also showed a possible understanding of our simulations on a microscopic ground and relationship between the parameters of the hybrid model and the parameters in these real systems (Appendix A). Experiments using polymer blends and block copolymers will be a good test for our theory and computer simulations.

Another important feature of the surfactant system which we did not discuss in this article is the effect of the spontaneous curvature.[11] If the surfactant molecule is not symmetric with respect to its two chemically distinct parts, such as head and tail of a soap molecule, the surfactant–adsorbed interface in general has a spontaneous curvature. Due to this spontaneous curvature, a transition from a bicontinuous structure to a micellar structure is expected. Such an effect can easily be incorporated into our hybrid model and simulation taking the spontaneous curvature into account is now under way.[12]

An extension to the three-dimensional case is another important future direction of the present study, where the hydrodynamic interaction plays an essential role. As the results of such simulations can directly be compared with the experimental results, they would provide helpful information in refining our model. In order to perform a quantitative comparison between the simulation results and those of real experiments, the molecular size as well as the excluded volume of the surfactant molecule should be taken into account in a proper manner.

Finally, we briefly discuss possible applications of the hybrid model to other problems than that discussed in the present paper. The essential point of the hybrid model is that the model is constructed on a mesoscopic level, where the system is partially coarse grained retaining some microscopic/mesoscopic degrees of freedom. For example, in the present problem of phase separation dynamics, the size and the shape of the surfactant molecule are taken into account. Such a molecular feature can play an important role in the macroscopic phase separation dynamics. One example is the nucleus effect of the surfactant molecule which initiates the phase separation in a metastable binary mixture and also accelerates the early stage phase separation in an unstable mixture.[4,6] Another example is the spontaneous curvature of the surfactant–adsorbed interfaces when the surfactant molecule has an asymmetric molecular shape.[12] These problems may also be treated by fully continuum approaches where the surfactant is also described by a continuous density field[9,10,41] with some additional supplementary fields, e.g., the director vector field of the surfactant molecules.[10,41] However, in such approaches, one has to adopt phenomenological assumptions on the static/dynamic features of such supplementary fields. Our hybrid approach will also be used to provide microscopic explanations of such phenomenological assumptions.

We also believe that the hybrid approach can be a suitable method to describe systems like complex fluids where large scale phenomena and small scale phenomena coexist. For example, one can consider the dynamics of a protein molecule in water, where the protein molecule is folded like a coil with some bridges made by sulfur atoms. There are two different length scales in this system; one is the gyration radius of the protein molecule, and the other is the length scale of the sulfur bridges and water molecules. Such a separation of length scales may be a target of the hybrid description. For example, one can treat the sulfur bridge and the water molecules around the bridge as a microscopic object while the other parts of the protein molecule and the water distant from the bridge are treated as continuum background. Such extension is one of the future directions of our hybrid model.

ACKNOWLEDGMENTS

One of the authors (T.K.) would like to thank M. Ernst, H. Frost, K. Fuchizaki, G. Gorecki, T. Hashimoto, K. Kaski, T. Koga, A. Nakahara, and W. Zimmermann for fruitful discussions and comments. Computations were performed at the Computer Centers of National Laboratory for High Energy Physics, Institute for Molecular Science and Kyushu University. The hospitality that T.K. received at these institutes are also acknowledged. This work is also supported by a Grant-in-Aid for Scientific Research on Priority Areas, "Computer Physics as a New Frontier in Condensed Matter Research," from the Ministry of Education, Science and Culture, Japan.

APPENDIX A

In this Appendix, we give a possible understanding of the hybrid model on a microscopic ground using a binary mixture and an amphiphilic block copolymer. (A similar problem is also discussed by Matsen and Schick.[42]) The discussion given below is also valid for a homopolymer mixture containing block copolymer chains, whose chain length is much larger than those of the homopolymer chains.

First, we consider the three-dimensional system. (An analogous argument for a two-dimensional system is given later.) We consider an A/B binary solvent mixture containing an A–B block copolymer which is composed of the same monomers as those of the A/B-mixture. For simplicity, we assume that the A-solvent and the B-solvent have the same size and also assume that the polymerization index of the block copolymer chain, N, is so large that de Gennes's scaling argument can be applicable to the chain

conformation.[3] (When we consider the homopolymer/block copolymer system, the word "solvent molecule" should be read as "homopolymer molecule" and the block copolymer chain should be regarded as a chain of blobs, whose radius of gyration is the same as that of the homopolymer chain. Then the argument is completely parallel.)

Let the linear dimension of the monomer (A/B solvent) be b, then the system can be described by a lattice Ising model with a lattice constant b with nearest neighbor interactions. In such a description, each A/B solvent molecule corresponds to one lattice site and a block copolymer chain is described by a linear chain of N_A A-monomers and N_B B-monomers ($N_A+N_B\equiv N$). We denote the interaction energies of $A-A$, $B-B$, and $A-B$ nearest neighbor pairs as $k_BT\chi_{AA}$, $k_BT\chi_{BB}$, and $k_BT\chi_{AB}$, respectively.

Using the local monomer number densities of A and B monomers of the solvent at the position $\mathbf{r}$, denoted as $\rho_A(\mathbf{r})$ and $\rho_B(\mathbf{r})$, the order parameter $X(\mathbf{r})$ is defined as

$$X(\mathbf{r})=\frac{1}{\rho_0}[\rho_A(\mathbf{r})-\rho_B(\mathbf{r})], \tag{A1}$$

where $\rho_0\equiv\rho_A+\rho_B(=1/b^3)$ is the total monomer number density. We neglected the volume fraction of the block copolymer. A mean field approximation for the binary solvent mixture gives the following free energy functional:[6]

$$\begin{aligned}H_{XX}=k_BT\int d\mathbf{r}[\rho_A(\mathbf{r})\ln\rho_A(\mathbf{r})+\rho_B(\mathbf{r})\ln\rho_B(\mathbf{r})]\\ +\frac{zk_BT}{2\rho_0}\int d\mathbf{r}\{\chi_{AA}[\rho_A(\mathbf{r})]^2\\ +2\chi_{AB}\rho_A(\mathbf{r})\rho_B(\mathbf{r})+\chi_{BB}[\rho_B(\mathbf{r})]^2\}+\cdots,\end{aligned} \tag{A2}$$

where z is the number of nearest neighbor sites and the ellipsis stands for the contribution from the spatial inhomogeneity of the composition (so-called gradient term). Expressing ρ_A and ρ_B in terms of ρ_0 and $X(\mathbf{r})$ and expanding the equation with respect to $X(\mathbf{r})$ ($|X(\mathbf{r})|\ll 1$), we obtain

$$H_{XX}=\frac{\rho_0k_BT}{8}\int d\mathbf{r}\left[\hat{D}_X(\nabla X)^2-\epsilon X^2+\frac{2}{3}X^4\right], \tag{A3}$$

where $\epsilon\equiv -4-z(\chi_{AA}+\chi_{BB}-2\chi_{AB})$ is the temperature distance from the mean field critical point. In Eq. (A3), we added the gradient contribution (the first term) with an empirical coefficient $\hat{D}_X$ whose explicit expression can be given by the density–density correlation function.[6]

Next, we consider the block copolymer chain. As the block copolymer chain is so long, the $A(B)$-subchain of the block copolymer can be regarded as a cloud of $A(B)$ monomers distributed symmetrically around the center of the subchain. The density distribution of such a cloud is given by the de Gennes theory for a swollen chain of polymerization index Z solubilized in a good solvent, and is denoted as $\psi_Z(r)$ with a normalization condition $\int\psi_Z(r)d\mathbf{r}=Z$.[3] Thus, the monomer density distribution of the ith block copolymer is given by

$$\begin{aligned}\phi_A^{(i)}(\mathbf{r})=\psi_{N_A}[|\mathbf{r}-\mathbf{r}_A^{(i)}|],\\ \phi_B^{(i)}(\mathbf{r})=\psi_{N_B}[|\mathbf{r}-\mathbf{r}_B^{(i)}|],\end{aligned} \tag{A4}$$

where $\mathbf{r}_A^{(i)}$ and $\mathbf{r}_B^{(i)}$ are the centers of the A-subchain and the B-subchain of the ith block copolymer. Then the interaction energy between the binary solvent mixture and the ith block copolymer is given by

$$\begin{aligned}H_{XS}^{(i)}=\frac{zk_BT}{4}\int d\mathbf{r}X(\mathbf{r})[\chi_A\phi_A(\mathbf{r})-\chi_B\phi_B(\mathbf{r})]\\ +\text{const},\end{aligned} \tag{A5}$$

where we introduced $\chi_A\equiv\chi_{AA}-\chi_{AB}$ and $\chi_B\equiv\chi_{BB}-\chi_{AB}$. The constant in Eq. (A5) can be incorporated into the chemical potential of the block copolymer and therefore can be dropped. Now the block copolymer is expressed as a pair of interaction centers, $\mathbf{r}_A^{(i)}$ and $\mathbf{r}_B^{(i)}$. Adopting the same dipole expansion for the block copolymer as was done in deriving the original version of the hybrid model[4] leads to a similar expressions for H_{XS} as before

$$\begin{aligned}H_{XS}=\frac{zk_BT}{4}\int d\mathbf{r}\left\{[\chi_A\psi_{N_A}(|\mathbf{r}-\mathbf{r}_i|)-\chi_B\psi_{N_B}(|\mathbf{r}-\mathbf{r}_i|)]X(\mathbf{r})+\left[\chi_A\psi_{N_A}(|\mathbf{r}-\mathbf{r}_i|)\frac{N_B}{N}+\chi_B\psi_{N_B}(|\mathbf{r}-\mathbf{r}_i|)\frac{N_A}{N}\right]l_i\hat{\mathbf{s}}_i\cdot\nabla X(\mathbf{r})\right.\\ \left.+\frac{1}{2}\left[\chi_A\psi_{N_A}(|\mathbf{r}-\mathbf{r}_i|)\left(\frac{N_B}{N}\right)^2-\chi_B\psi_{N_B}(|\mathbf{r}-\mathbf{r}_i|)\left(\frac{N_A}{N}\right)^2\right]l_i^2\hat{\mathbf{s}}_i\hat{\mathbf{s}}_i:\nabla\nabla X(\mathbf{r})+\cdots\right\},\end{aligned} \tag{A6}$$

where l_i is the distance between $\mathbf{r}_A^{(i)}$ and $\mathbf{r}_B^{(i)}$, and $\hat{\mathbf{s}}_i$ is the director vector of the ith block copolymer chain defined as the unit vector along $\mathbf{r}_A^{(i)}-\mathbf{r}_B^{(i)}$. The dipole expansion used in deriving Eq. (A6) is valid when the field $X(\mathbf{r})$ does not change appreciably over the distance l_i, that is $l_i|\nabla X|\ll 1$. In the simulations of the hybrid model, this condition is sometimes violated, especially in the late stage, because we assumed that the size of the surfactant molecule (block copolymer chain) is the same order as the correlation length of the binary mixture, the latter corresponding to the interfacial thickness. Thus, we would have to take not only the dipole but also the multipoles into account to get

a quantitative results. However, at the present stage, we are interested only in the qualitative features of the surfactant system, which are well be reproduced by the dipole approximation.

Now we adopt the following approximated form for $\psi_Z(r)$:[43]

$$\psi_Z(r)=\frac{2Z}{\bar{R}_Z^3}\exp\left[-\frac{1}{2}\left(\frac{r}{\bar{R}_Z}\right)^2\right], \tag{A7}$$

where $\bar{R}_Z=bZ^{3/5}$ is the so-called Flory radius for a chain in an athermal solvent. Then the parameter l_i can be expressed as $l_i=b(N/2)^{3/5}$. The expression for H_{SS} can also be obtained in a similar manner, but we do not show it here explicitly.

Next we consider the kinetic coefficients. The kinetic coefficients L^X, L^ρ, and L^s can be described by the solvent diffusion coefficient D_1. The kinetic coefficient for the field $X(\mathbf{r})$ appears in the TDGL equation

$$\frac{\partial}{\partial t}X=L^X\nabla^2\frac{\delta H_{XX}}{\delta X}. \tag{A8}$$

Substituting Eq. (A3) into Eq. (A8) and linearizing with respect to X, we obtain a diffusion equation for X in the long wave length limit. If we consider the high temperature region where the difference between A and B component disappears, i.e., $\epsilon=-4$ ($\chi_{AA}=\chi_{BB}=\chi_{AB}$), the diffusion coefficient of such a diffusion equation can be identified with the self-diffusion coefficient, D_1, and we find $L^X=D_1/\rho_0 k_B T$. On the other hand, using the Rouse description for the block copolymer chain,[43] one finds that the kinetic coefficient for the translational motion of the block copolymer chain, L^ρ, is given by $L^\rho=D_1/Nk_BT$. The kinetic coefficient for the rotation of the block copolymer chain, L^s, is obtained by identifying the block copolymer chain as a rod of length l_i, and we obtain $L^s=12bD_1/l_i^3k_BT$.[43] The level of the thermal noises acting on the field $X(\mathbf{r})$ and the block copolymer can be related to these kinetic coefficients.

Taking the units of length, energy and X as $l_0\equiv(\hat{D}_X/\epsilon)^{1/2}$, $(3/16)\rho_0 k_B T\epsilon^2 l_0^3$ and $(3\epsilon)^{1/2}/2$, one finally obtains the same form as Eqs. (2.2)–(2.12), from which one can get the microscopic expressions for the parameters of the hybrid model.

Assuming the A–B symmetry of the system as was done in the simulation, the parameters in the hybrid model can be expressed in terms of the parameters of the microscopic lattice model as follows:

$$\begin{aligned}
&L^\rho/L^X=\frac{3\epsilon}{4N}\left(\frac{l_0}{b}\right)^3,\\
&L^s/L^X=9\cdot 2^{9/5}\epsilon N^{-9/5}\left(\frac{l_0}{b}\right)^5,\\
&\frac{ql}{2}V_0=\frac{2z\chi b}{3^{1/2}\epsilon^{3/2}l_0}\left(\frac{N}{2}\right)^{-1/5},\\
&\xi=\frac{bN^{3/5}}{l_0},\quad T=\frac{16}{3\epsilon^2}\left(\frac{b}{l_0}\right)^3,
\end{aligned} \tag{A9}$$

where we denoted $V_-(r)=V_0\exp[-(r/\xi)^2]$. Here, we note that the value of l_0 is the same as the correlation length and can be determined from the peak position of the scattering function in the linear regime.

For a two-dimensional version of the above argument, one can consider a binary homopolymer mixture containing a large block copolymer in a Helle–Shaw cell, i.e., a thin polymer layer between two glass plates placed parallel to each other.[44] When such a homopolymer/block copolymer mixture is filled within a pair of parallel glass plates with a separation distance d, which is the same order as the gyration radius of the homopolymer chain, the system can be regarded as essentially two-dimensional. The argument is almost similar to that for the three-dimensional system given above. The only difference is that one should use the radius of the homopolymer chain as the parameter b (lattice spacing) and regard the block copolymer chain as a linear chain of blobs of radius b.

One important effect which enters in this two-dimensional case is the preferential wetting between the two components of the binary mixture and the glass plates, which changes the morphology of the domain structure drastically and affects the coarsening process.[45] Similarly, surfactant molecules will also be adsorbed onto the glass plates. Such effects are essential in two-dimensional systems like the Helle–Shaw system and can be introduced into our hybrid model.

APPENDIX B

In order to solve the partial differential equation for the field $X(\mathbf{r})$, Eq. (2.2), we adopted the fully implicit method,[46] which is unconditionally stable for any time mesh width Δt. In solving the equation, we regarded the thermodynamic force coming from the cross coupling terms between the field $X(\mathbf{r})$ and the surfactant as an external force to the field X and only the evolution equation for the field X is treated implicitly. Resulting self-consistent equation is solved by the iteration method.

Although the scheme is unconditionally stable, a choice of a too large Δt causes an error in the computation.[46] We compared the results of the simulation using this implicit method with the results obtained by the explicit method with a sufficiently small Δt ($\Delta t=0.01$; the same value as that in our previous works[4–6]).[27] From this comparison, we confirmed that the qualitative features are unchanged even when the implicit scheme is used with a rather large value of Δt, i.e., $\Delta t=0.5$, and only the time scale is changed. In order to know the rescaling factor of time for different values of Δt, we calculated the maximum growth rate of the scattering function in the linear regime, 2λ, defined by

$$S(k_0,t)\sim\exp[2\lambda(k_0)t], \tag{B1}$$

where k_0 is the maximum peak position. We show the results in Fig. 17. One can see that the time is elongated by a factor 3.6 when one uses $\Delta t=0.5$.

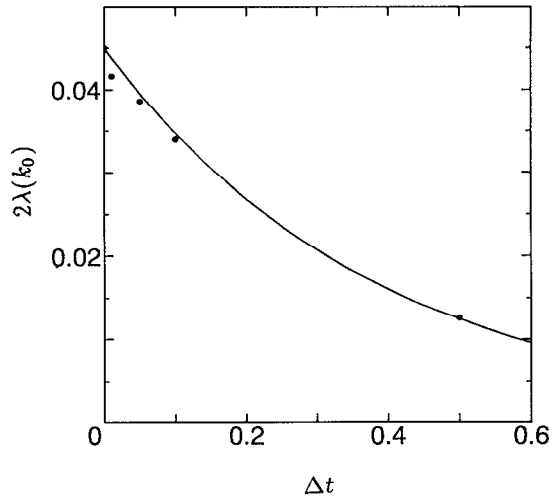

FIG. 17. Growth rate of the structure function in the linear regime plotted as a function of the time mesh width Δt.

APPENDIX C

In this Appendix, we describe how we calculated the curvature distributions and the micellar size distributions.

We define the interface as the line where $X(\mathbf{r})=0$. This line is composed of many sections of short straight lines with a length a, the space mesh size. Let the position of the mth section be R_m, m being the index of the section along the interface. Then, the curvature at a point on the interface is defined by the curvature of a circle going through the three points, R_m, R_{m-M}, and R_{m+M}. We also defined the length of the mth section by $1/(2Ma)$ of the arc length of the circle between the two points R_{m-M} and R_{m+M}. In this work, we chose the parameter M to be $M=10$, which was found to be appropriate to measure the curvature with a reasonable resolution and also to avoid the effects of the discreteness of the space mesh.

To calculate micellar size distribution function, we first defined the perimeter of a micelle in the same manner as above, i.e., by the line where $X(\mathbf{r})=0$. Then we regarded the micellar size as the radius of a circle whose enclosed area is equal to the enclosed area of the perimeter.

Above procedures to determine curvature and micellar size distributions are not appropriate for the system with thermal noise, because the interfaces are no longer smooth due to thermal agitation. In order to eliminate such a difficulty, we adopted a coarse-graining procedure, where the value of $X(\mathbf{r})$ at each mesh point is replaced by the averaged value over the four nearest neighbor mesh points and the mesh under consideration.

[1] *Dynamics and Patterns in Complex Fluids*, edited by A. Onuki and K. Kawasaki (Springer, Heidelberg, 1989).
[2] *Slow Dynamics in Condensed Matter*, edited by K. Kawasaki, M. Tokuyama, and T. Kawakatsu (American Institute of Physics, New York, 1992).
[3] P. G. de Gennes, *Scaling Concepts in Polymer Physics* (Cornell University, Ithaca, 1979).
[4] T. Kawakatsu and K. Kawasaki, Physica A **167**, 690 (1990).
[5] T. Kawakatsu and K. Kawasaki, in *Molecular Dynamics Simulations*, edited by F. Yonezawa (Springer, Berlin, 1992).
[6] T. Kawakatsu and K. Kawasaki, J. Colloid Interface Sci. **145**, 413 (1991); **145**, 420 (1991).
[7] T. Kawakatsu and K. Kawasaki, J. Colloid Interface Sci. **148**, 23 (1991). Another Monte Carlo simulation on the dynamics of surfactant systems using a lattice model is also reported in D. Moraietz, D. Chowdhury, S. Vollmar, and D. Stauffer, Physica A **187**, 126 (1992).
[8] T. Kawakatsu and K. Kawasaki, in *From Phase Transitions to Chaos*, edited by G. Györgyi, I. Kondor, L. Sasvári, and T. Tél (World Scientific, Singapore, 1992).
[9] M. Laradji, H. Guo, M. Grant, and M. Zuckermann, J. Phys. A **24**, L629 (1991); J. Phys. Condensed Matter **4**, 6715 (1992).
[10] A similar continuum model has also been proposed in K. Kawasaki and T. Kawakatsu, Physica A **164**, 549 (1990).
[11] D. J. Mitchell and B. W. Ninham, J. Chem. Soc. Faraday Trans. II **77**, 601 (1981).
[12] T. Kawakatsu *et al.* (unpublished).
[13] R. J. Roe and C. M. Kuo, Macromolecules **23**, 4635 (1990); D. W. Park and R. J. Roe, *ibid.* **24**, 5324 (1991).
[14] T. Hashimoto and T. Izumitani, Macromolecules **26**, 3631 (1993).
[15] T. Koga and K. Kawasaki, Phys. Rev. A **44**, R817 (1991).
[16] H. E. Cook, Acta Metall. **18**, 297 (1970).
[17] T. Hashimoto, in *Dynamics of Ordering Processes in Condensed Matter*, edited by S. Komura and H. Furukawa (Plenum, New York, 1988).
[18] P. Guenoun, R. Gastaud, F. Perrot, and D. Beysens, Phys. Rev. A **36**, 4876 (1987); D. Beysens, P. Guenoun, and F. Perrot, *ibid.* **38**, 4173 (1988).
[19] S. Puri and Y. Oono, J. Phys. A **21**, L755 (1988).
[20] M. P. Allen and D. J. Tildesley, *Computer Simulation of Liquids* (Oxford, New York, 1987).
[21] D. W. Heermann, *Computer Simulation Methods*, 2nd ed. (Springer, New York, 1990).
[22] Y. Oono and S. Puri, Phys. Rev. A **38**, 434 (1988).
[23] S. H. Anastasiadis, I. Gancarz, and J. T. Koberstein, Macromolecules **22**, 1449 (1989).
[24] K. Kawasaki and T. Ohta, Physica A **118**, 175 (1983).
[25] C. G. Vonk, J. F. Billman, and E. W. Kaler, J. Chem. Phys. **88**, 3970 (1988).
[26] N. Kuwahara and K. Kubota, Phys. Rev. A **45**, 7385 (1992).
[27] T. Kawakatsu, K. Kawasaki, M. Furusaka, H. Okabayashi, and T. Kanaya, KENS *Report* (KEK *Progress Report*) IX, 1993, p. 128.
[28] W. Helfrich, Z. Naturforsch. C **28**, 693 (1973).
[29] S. T. Milner, S. A. Safran, D. Andelman, M. E. Cates, and D. Roux, J. Phys. (France) **49**, 1065 (1988); P. Chandra and S. A. Safran, Europhys. Lett. **17**, 691 (1992).
[30] M. Teubner, J. Chem. Phys. **92**, 4501 (1990).
[31] P. G. deGennes and C. Taupin, J. Phys. Chem. **86**, 2294 (1982).
[32] J. Noolandi and K. M. Hong, Macromolecules **17**, 1531 (1984).
[33] D. J. Srolovitz and G. N. Hassold, Phys. Rev. B **35**, 6902 (1987).
[34] T. M. Rogers and R. C. Desai, Phys. Rev. B **39**, 11 956 (1989).
[35] J. H. Yao, K. R. Elder, H. Guo, and M. Grant, Phys. Rev. B **45**, 8173 (1992).
[36] R. Toral, A. Chakrabarti, and J. D. Gunton, Phys. Rev. A **45**, R2147 (1992).
[37] I. M. Lifschitz and V. V. Slyozov, J. Phys. Chem. Solids **19**, 35 (1961).
[38] G. Brown and A. Chakrabarti, J. Chem. Phys. **98**, 2451 (1993).
[39] T. Hashimoto, M. Takenaka, and H. Jinnai, J. Appl. Crystallogr. **24**, 457 (1991).
[40] E. Siggia, Phys. Rev. A **20**, 595 (1979).
[41] G. Gompper and S. Klein, J. Phys. II (France) **2**, 1725 (1992).
[42] M. W. Matsen and M. Schick (preprint).
[43] M. Doi and S. F. Edwards, *The Theory of Polymer Dynamics* (Oxford Science, New York, 1986).
[44] A. Shinozaki and Y. Oono, Phys. Rev. A **45**, R2161 (1992).
[45] J. Bodensohn and W. I. Goldburg, Phys. Rev. A **46**, 5084 (1992).
[46] W. H. Press, B. P. Flannery, S. A. Teukolsky, and W. T. Vetterling, *Numerical Recipes in C* (Cambridge University, Cambridge, 1988).